2019-03-10

Uniaxial Damaged Plastic Constitutive Relation of Recycled Aggregate Concrete

Hu, X

10.1155/2019/2982195
Advances in Materials Science and Engineering
Hindawi

Hindawi
Advances in Materials Science and Engineering
Volume 2019, Article ID 2982195, 16 pages
https://doi.org/10.1155/2019/2982195

Research Article

Uniaxial Damaged Plastic Constitutive Relation of Recycled Aggregate Concrete

Xiaobin Hu[1], **Qinwang Lu**[1] and **Shanshan Cheng**[2]

[1]*School of Civil Engineering, Wuhan University, Wuhan 430072, China*
[2]*School of Engineering, University of Plymouth, Plymouth PL4 8AA, UK*

Correspondence should be addressed to Shanshan Cheng; shanshan.cheng@plymouth.ac.uk

Received 10 January 2019; Accepted 25 February 2019; Published 10 March 2019

Academic Editor: Aniello Riccio

This paper presents a proposed uniaxial damaged plastic constitutive relation of recycled aggregate concrete (RAC) based on the experimental studies. A total of five groups of RAC specimens with different recycled coarse aggregate (RCA) replacement percentages of 0, 25%, 50%, 75%, and 100%, respectively, are tested under both monotonic loading and cyclic loading. The effect of the RCA replacement percentage is thoroughly investigated on a variety of mechanical properties, including the compressive strength, the peak strain, and the elastic modulus. Based on the test results, a uniaxial damage plastic constitutive relation of the RAC is proposed within the continuous thermodynamics framework. After validated by the experimental results, the proposed damaged plastic constitutive relation of the RAC is applied to perform nonlinear analysis of the RAC columns under cyclic loading, which provides close predictions of the hysteresis behavior of the RAC columns.

1. Introduction

Due to rapid urbanisation in recent years, the engineering construction grows substantially worldwide, particularly in China. A large amount of waste concrete has been produced due to the renovation or demolition of existing buildings, which occupies a lot of land and may have a detrimental impact on the surrounding environment. Therefore, how to dispose the waste concrete has become an important issue. The recycled aggregate concrete (RAC) technology emerges as an effective way to reuse the waste concrete and thus attracts a lot of interests from the scholars and engineers [1]. The RAC is mainly made of the recycled coarse aggregate (RCA) and/or natural coarse aggregate (NCA), natural fine aggregate, cement binder, and water. Compared with the NCA, the RCA generally has smaller apparent density, larger water absorption, and lower strength due to the inner damage resulted from the crushing process of the waste concrete [2, 3].

Extensive experimental studies have been conducted concerning the compressive performance of the RAC. Some researchers [4–9] found that the strength and elastic modulus of the RAC decrease while the deformation capacity increases with the increase in the RCA replacement percentage. However, other researchers [10–15] draw contrary conclusions. They found that the strength of the RAC gets improved with the increase in the RCA replacement percentage, which is because that the high water absorption rate of the RCA reduces the effective water participation in the cement hydration reaction, and thereby causes a lower effective water-cement ratio. In addition, some other researchers [16, 17] declared that the strength of the RAC does not change monotonically with the increase in the RCA replacement percentage.

In addition to the above studies, only a few scholars investigated the compressive stress-strain relation of the RAC and proposed the corresponding constitutive model. Bairagi et al. [18] presented the ascending branch of the uniaxial compressive stress-strain curve of the RAC. They found that both peak stress and curvature of the ascending branch of the curve increase with the increase in the RCA replacement percentage. Similar researches have been

performed by other researchers [5, 12, 19], where the full uniaxial stress-strain relation of the RAC under compression has been obtained. It is also found that increasing the RCA replacement percentage decreases the ductility as the descending branch of the stress-strain curve becomes steeper. By simply fitting the experimental curves, various constitutive relations of the RAC have been proposed [5, 12, 19]. However, the relevant studies are mainly focused on monotonic loading, whereas the mechanical properties of the RAC under cyclic loading remain unclear.

In recent decades, the continuum damage mechanics has been widely used to describe the nonlinear mechanical performance of the natural aggregate concrete (NAC). The proposed damage constitutive model appears to be capable of capturing well the key mechanical properties of the NAC, e.g., the stress softening in compression and the stiff degradation when unloading [20–23]. Motivated by this method, this study is conducted mainly to propose the damaged plastic constitutive model of the RAC within continuous thermodynamics framework. To achieve this goal, a total of five groups of RAC specimens with different RCA replacement percentages are tested under both monotonic loading and cyclic loading. Based on the experimental results, the formulae are established for calculating the key mechanical properties, including the compressive strength, the peak strain, and the elastic modulus, as well as the plastic strain and the damage variable. After validated by experimental results, the proposed damaged plastic constitutive model of the RAC is further applied in the nonlinear analysis of the RAC columns subjected to cyclic loading.

2. Experimental Investigation of the RAC

2.1. Specimen Design. For the RAC in this test, ordinary Portland cement with a 28 d compressive strength of 42.5 MPa is used. The fine aggregate is river sand, and the RCA is obtained by crushing the waste concrete specimens collected from the local quality inspection station. The compressive strength of the waste concrete specimens ranges from 30 MPa to 50 MPa.

The main physical properties of the coarse aggregate are summarized and listed in Table 1. The ratios between the physical properties of the RCA and NCA are given as well. It can be clearly seen that the bulk density and apparent density of the RCA are smaller than those of the NCA, while the water absorption and crush index are substantially larger. It can be attributed to the presence of old mortar surrounded around the RCA. For both RCA and NCA, the grain sizes fall between 5 mm and 31.5 mm. Figure 1 plots the grading curves of the RCA and NCA, as well as the upper and lower bound specified in the code DG/TJ08-2018-2007 [25], which shows that both are continuously graded and satisfy the code requirement.

In order to investigate the influence of the RCA replacement percentage on the mechanical performance of the RAC, a total of five groups of specimens are prepared using five different replacement percentages, i.e., 0%, 25%, 50%, 75%, and 100%. Note that the RAC placement percentage is

Table 1: Main physical properties of the coarse aggregate.

Type	Bulk density ($kg \cdot m^{-3}$)	Apparent density ($kg \cdot m^{-3}$)	Water absorption (%)	Crush index (%)
NCA	1423	2810	0.56	6.7
RCA	1281	2506	4.2	15.5
Ratio	0.90	0.89	7.5	2.3

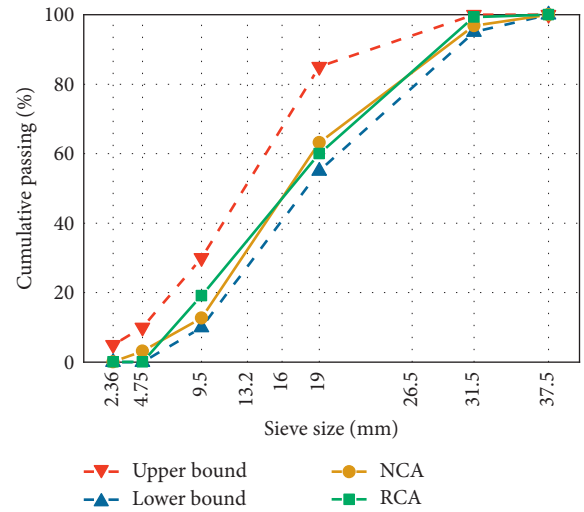

Figure 1: Grading curves of the coarse aggregates (reproduced from Hu et al. [24] (under the Creative Commons Attribution License/public domain)).

defined as the ratio between the RCA weight and the total coarse aggregate weight. In the case of 0%, the RAC turns to the NAC. Each group includes three cube specimens with the size of 150 mm × 150 mm × 300 mm and six prism specimens with the size of 150 mm × 150 mm × 300 mm. The cube specimens are used to obtain the cubic compressive strength. The prism specimens are intended to measure the stress-strain curves of the RAC, among which three are tested under monotonic loading and the other three are tested under cyclic loading.

The mix proportions of the RAC are determined according to the code DG/TJ08-2018-2007 [26]. Considering the high water absorption of the RCA, which reduces the effective water-cement ratio in the RAC and therefore exerts great impact on the mechanical performance of the RAC [17, 27, 28], additional water is used in this study. Table 2 gives the mix proportions of the RAC corresponding to different replacement percentages, where the number in the first column denotes the RCA replacement percentage.

2.2. Test Scheme. The specimens were water-cured under laboratory conditions for 28 days and were tested using the Instron electrohydraulic servo test machine as shown in Figure 2. In the monotonic test, the displacement loading rate was kept as 0.02 mm/s, which corresponds to a strain rate of 67×10^{-6}/s. Unlike the monotonic test, the hybrid loading scheme was adopted for the cyclic test. For each cycle, the specimen was first loaded with the strain rate of

Table 2: Mix proportions of the RAC (reproduced from Hu et al. [24] (under the Creative Commons Attribution License/public domain)).

No.	Replacement percentage	Cement (kg/m^3)	Sand (kg/m^3)	NCA (kg/m^3)	RCA (kg/m^3)	Water (kg/m^3)	Additional water (kg/m^3)
NAC	0	430	618	1200	0	185	0
RAC-25	25	430	607	883	295	185	12.4
RAC-50	50	430	595	578	578	185	24.3
RAC-75	75	430	585	284	851	185	35.7
RAC-100	100	430	574	0	1114	185	46.8

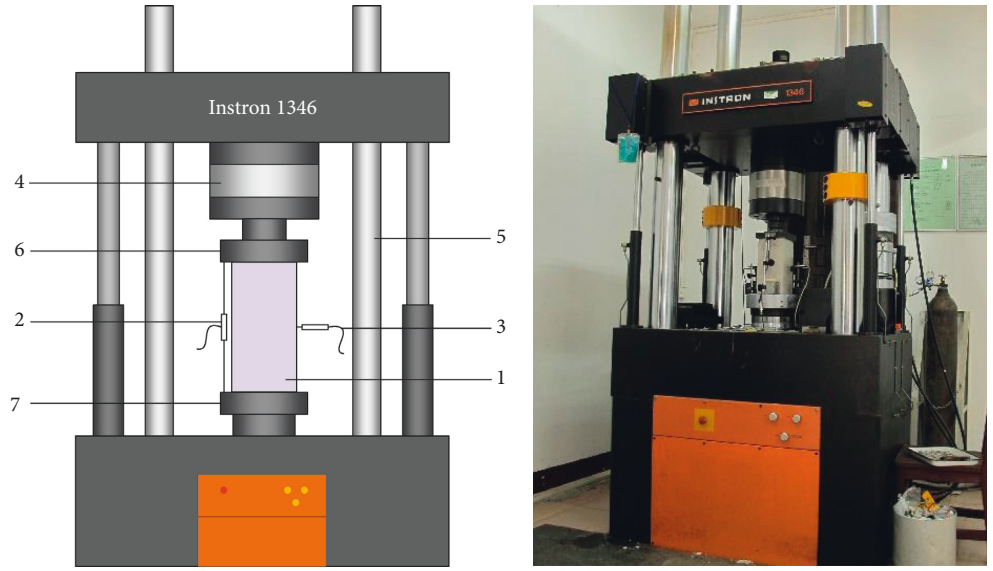

(1) Specimen
(2) Longitudinal displacement sensor
(3) Transverse displacement sensor
(4) Force sensor
(5) Rigid auxiliary frame
(6) Top backing plate
(7) Bottom backing plate

(a) (b)

Figure 2: Test setup. (a) Schematic diagram. (b) Test photo.

67×10^{-6}/s and then unloaded at the rate of 10 kN/s until the load is zero. The maximum strain at each cycle was increased by about 1×10^{-3} up to the failure of the specimen. The other relevant details can be seen in reference [24].

As shown in Figure 2, the axial force acted on the specimen was obtained by the force transducer, and the longitudinal and transverse displacements were measured using the displacement sensor. The corresponding axial stress and strain are determined as follows:

$$\sigma^{\mathrm{r}} = \frac{N}{A}, \qquad \varepsilon^{\mathrm{r}} = \frac{\Delta l}{l}, \tag{1}$$

where σ^{r} and ε^{r} are the stress and strain of the RAC, respectively; N and Δl represent the measured axial force and displacement, respectively; and A and l are the cross-sectional area and length of the specimen, respectively.

2.3. Test Result

2.3.1. Compressive Strength. For all specimens, the measured compressive strengths are listed in Table 3, where f_{cu} represents the cube compressive strength, $f_{\mathrm{c},1}$ is the prism compressive strength under cyclic loading, and $f_{\mathrm{c},2}$ is the prism compressive strength under monotonic loading. Note that the value is averaged over the three specimens with the same parameters.

Figure 3 shows the average cube compressive strength of the RAC for different RCA replacement percentages and the average prism compressive strength under cyclic loading and monotonic loading, respectively, where r denotes the RCA replacement percentage. It can be seen that, on the whole, the compressive strength of RAC first decreases and then increases as the RCA replacement percentage increases. This nonmonotonic variation trend was also observed by other researchers [15–17]. It can be resulted from the experimental randomness or the intricate interaction

Table 3: Main mechanical properties of the RAC.

No.	Compressive strength (MPa)			Peak strain (10^{-3})		Elastic modulus (GPa)		Secant modulus (GPa)	
	f_{cu}	$f_{c,1}$	$f_{c,2}$	$\varepsilon_{c,1}$	$\varepsilon_{c,2}$	$E_{c,1}$	$E_{c,2}$	$E_{s,1}$	$E_{s,2}$
NAC	31.14	27.40	24.59	1.95	1.96	31.58	28.85	14.05	12.55
RAC-25	32.48	27.50	26.81	2.03	2.11	30.49	28.76	13.54	12.71
RAC-50	29.22	22.92	24.19	2.09	2.09	25.01	27.12	10.97	11.57
RAC-75	37.28	26.94	27.53	2.32	2.23	26.63	28.00	11.61	12.35
RAC-100	38.05	28.78	27.84	2.54	2.41	25.20	26.12	11.33	11.55

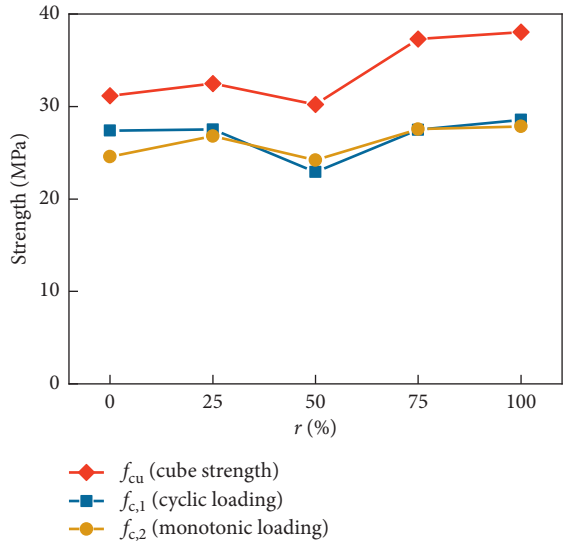

Figure 3: Compressive strength of the RAC.

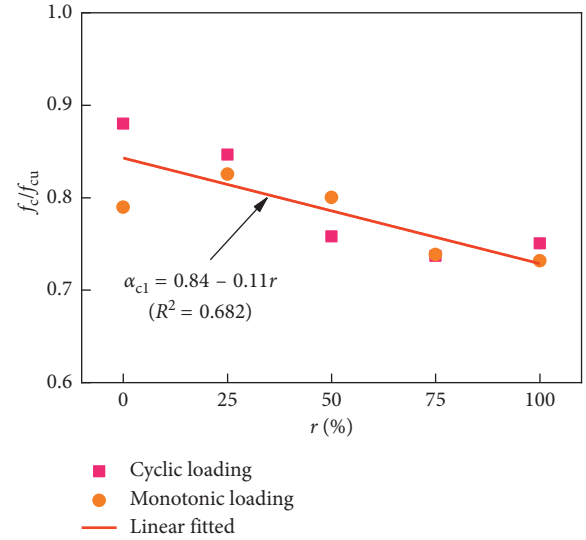

Figure 4: Relation between the prism compressive strength and cube compressive strength.

mechanism between the RCA and NCA, which needs to be further investigated in the future study. In addition, it is found that, for the same RCA replacement percentage, the prism samples provide close compressive strength under both monotonic loading and cyclic loading, but the cube samples provide higher compressive strength than the prism samples as a result of the size effect.

Figure 4 plots the ratios of compressive strength between the prism samples and the cubic samples corresponding to different RCA replacement percentages. It can be seen that the ratio generally decreases with the increase in the RCA replacement percentages, indicating that the size effect on the RAC strength appears more pronounced as the content of the RCA increases. It can be explained that the RCA has lower strength and lower interlock capacity between aggregates compared to the NAC because the RCA has more inner damages caused during the crushing process. Therefore, as the RCA replacement percentage increases, the RCA has more disadvantageous influence on the strength of the prism specimen compared to the cube specimen since the former has a larger amount of RCA due to its larger size.

Suppose that α_{c1} is the ratio between the prism compressive strength and cubic compressive strength, i.e.,

$$f_c = \alpha_{c1} f_{cu}. \tag{2}$$

Based on the experimental results, the following equation could be obtained using regression analysis:

$$\alpha_{c1} = 0.84 - 0.11r. \tag{3}$$

2.3.2. Peak Strain. Table 3 also gives the average peak strain corresponding to the peak stress, where $\varepsilon_{c,1}$ and $\varepsilon_{c,2}$ denote the peak stain under cyclic loading and monotonic loading, respectively. Figure 5 shows the peak strain corresponding to different RCA replacement percentages. It can be seen that the peak strain generally increases as the RCA replacement percentages increases. For example, as r changes from 0% to 100%, $\varepsilon_{c,1}$ and $\varepsilon_{c,2}$ increase by about 29% and 23%, respectively. This finding is consistent with that from some other researchers [5, 19, 29, 30]. The increase in the peak strain with the increase in the RCA replacement percentage is mainly due to the reduced elastic modulus of the RCA [5, 19, 30].

To approximately estimate the peak strain of the NAC from the compressive strength, the European standard BS EN 1992-1-1 [31] and the Chinese standard GB50010-2010 [32] give the following relations, respectively:

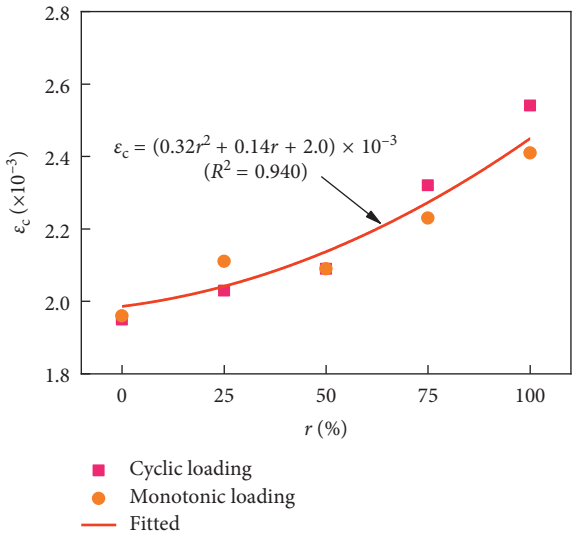

Figure 5: Effect of the RCA replacement percentage on the peak strain.

$$\varepsilon_c = \left(0.7 f_{cm}^{0.31}\right) \times 10^{-3}, \tag{4a}$$

$$\varepsilon_c = \left(0.7 + 0.172\sqrt{f_c}\right) \times 10^{-3}, \tag{4b}$$

where f_{cm} is the cylinder compressive strength and can be set as $0.80 f_{cu}$ in the absence of test data. Referring to the above equations, the following similar relations are assumed for the RAC.

$$\varepsilon_c = \alpha_\varepsilon \left(0.7 f_{cm}^{0.31}\right) \times 10^{-3}, \tag{5a}$$

$$\varepsilon_c = \alpha_\varepsilon \left(0.7 + \left(0.172\sqrt{f_c}\right)\right) \times 10^{-3}, \tag{5b}$$

where α_ε is the coefficient to consider the influence of the RCA replacement percentages.

Using the above two equations, the values of α_ε corresponding to different RCA replacement percentages can be obtained based on the experimental results. It can be seen in Figure 6 that α_ε generally ascends linearly with the increase in the RCA replacement percentage. Through regression analysis, the following relations regarding equations (5a) and (5b) can thus be established, respectively:

$$\alpha_\varepsilon = 0.23r + 1.01, \tag{6a}$$

$$\alpha_\varepsilon = 0.28r + 1.23. \tag{6b}$$

The fitting curves are also shown in Figure 6. It can be seen that equations (5a) and (5b) both yield a satisfactory estimate of the peak strain of the RAC based on its compressive strength.

2.3.3. Elastic Modulus. Table 3 also lists the average elastic modulus and secant modulus, where E_{c1} and E_{c2} represent the elastic modulus under cyclic loading and monotonic loading, respectively, while E_{s1} and E_{s2} are the secant modulus corresponding to the peak point on the stress-strain curve under cyclic loading and monotonic loading, respectively. In this study, the elastic modulus is taken as the secant slope at the point on the stress-strain curve where the stress equals $0.4 f_c$.

Figure 7 shows the elastic modulus of the RAC corresponding to different RCA replacement percentages. It can be seen that the elastic modulus generally decreases with the increase in the RCA replacement percentage. It is similar to the observations made by other researchers [6, 7], which is mainly attributed to that more inner defects exist in the RCA compared to that in the NCA. In addition, Figure 8 shows the relation between the elastic modulus and secant modulus of the RAC. It can be found that the ratio between the two modulus ranges between 2.2 and 2.4, irrespective of the RCA replacement percentage.

For the NAC, the European standard BS EN 1992-1-1 [31] gives the following relation between the elastic modulus and compressive strength:

$$E_c = 22\alpha_E \left(\frac{f_{cm}}{10}\right)^{0.3} \text{(GPa)}, \tag{7}$$

where α_E is the coefficient to account for the influence of the coarse aggregate type. The above equation is extended in this study to establish the relation between the elastic modulus and compressive strength for the RAC, where α_E is redefined as the coefficient to reflect the influence of the RAC replacement percentage. Similarly, the Chinese standard GB50010-2010 [32] also provides the formula of calculating the elastic modulus from the compressive strength for the NAC as follows:

$$E_c = \frac{10^5}{(2.2 + 34.7/f_{cu})} \text{(MPa)}. \tag{8}$$

By introducing the coefficient α_E, the following equation can be also formulated to describe the relation between the elastic modulus and the compressive strength for the RAC:

$$E_c = \alpha_E \frac{10^5}{(2.2 + 34.7/f_{cu})} \text{(MPa)}. \tag{9}$$

Utilizing equations (7) and (9), the values of α_E corresponding to different RCA replacement percentages can be obtained using the experimental data. It can be seen in Figure 9 that α_E generally drops with the increase in the RCA replacement percentage. By regression analysis, the following relations corresponding to equations (7) and (9) can be established:

$$\alpha_E = -0.17r + 1.03, \tag{10a}$$

$$\alpha_E = -0.20r + 1.00. \tag{10b}$$

2.3.4. Stress-Strain Curve. The stress-strain curves averaging over the three specimens corresponding to different RCA replacement percentages under cyclic and monotonic loading are shown in Figures 10(a)–10(e). The skeleton curves pertaining to the stress-strain curves under cyclic

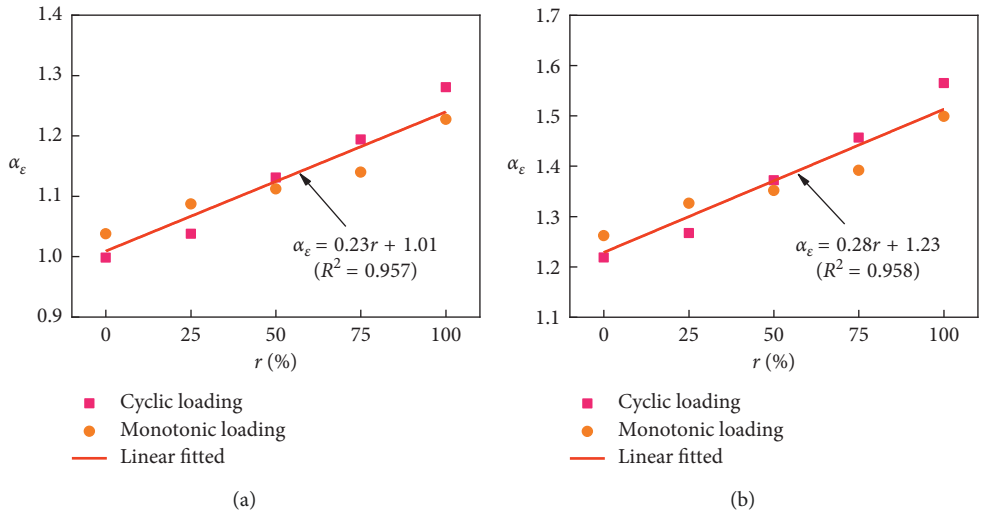

Figure 6: Effect of the RCA replacement percentage on the values of α_ε corresponding to (a) equation (5a) and (b) equation (5b).

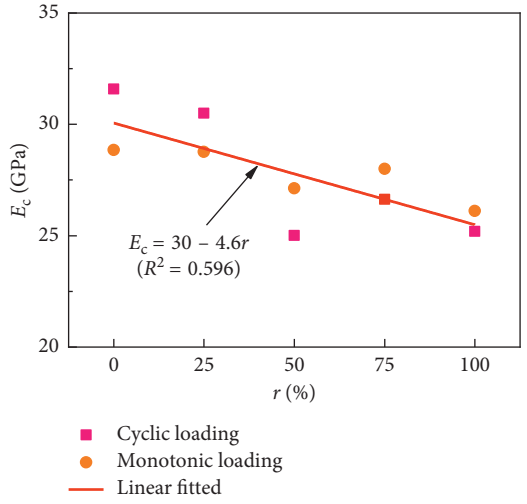

Figure 7: Effect of the RCA replacement percentage on the elastic modulus.

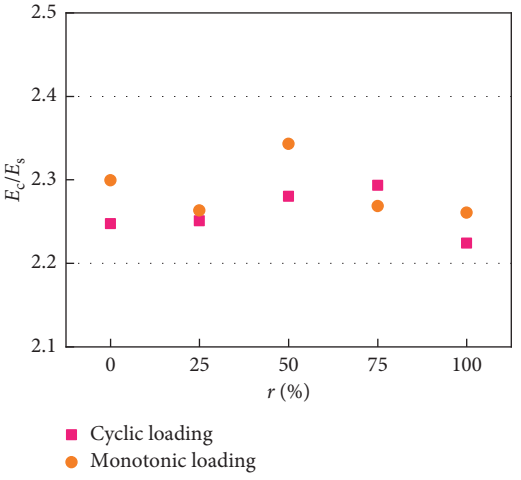

Figure 8: Relations between elastic modulus and secant modulus.

loading are also plotted in these figures, which are obtained by connecting the peak point of each hysteresis loop. It can be seen that the skeleton curve under cyclic loading is close to the stress-strain curve under monotonic loading. Furthermore, as the RCA replacement percentage increases, the discrepancy tends to be even smaller.

To further investigate the effect of the RCA replacement percentage on the stress-strain curve, these skeleton curves are plotted all together in Figure 10(f). It is observed that these curves nearly coincide when the stress is relatively small (<16 MPa), showing that the RCA replacement percentage has little effect on the ascending branch of the curves, especially in the elastic range. However, beyond the elastic range, obvious difference can be found on the curves in terms of the peak stress and descending branch. In general, similar to the NAC, the higher the peak stress of the RAC, the steeper the descending branch of the skeleton curves.

In addition, it can be seen from the hysteresis curves under cyclic loading that the average slope of unloading branch or the reloading branch decreases as the strain at the unloading point or reloading point increases. It can be attributed to the development of damage resulted from the propagation of inner microcracks in the specimens. Moreover, it is worth noting that the average slope of an unloading branch is close to that of the subsequent reloading branch.

3. Uniaxial Damaged Plastic Constitutive Relation of the RAC

3.1. Formulation of the General Uniaxial Damaged Plastic Constitutive Relation. For the isotropic material under uniaxial stress, the total strain can be written as the sum of the elastic strain and plastic strain as follows:

$$\varepsilon = \varepsilon^e + \varepsilon^p, \tag{11}$$

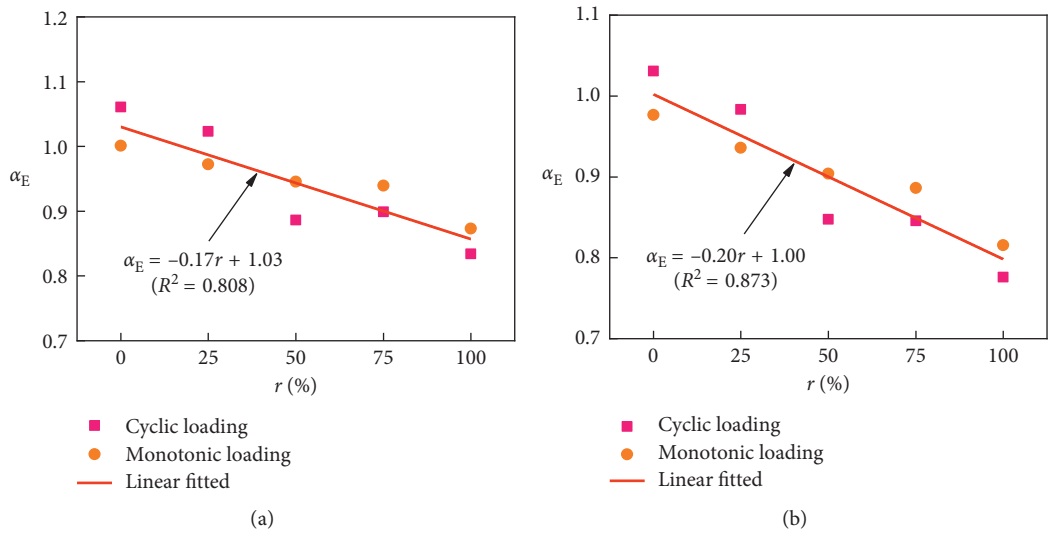

Figure 9: Effect of the RCA replacement percentage on the values of α_E corresponding to (a) equation (7) and (b) equation (9).

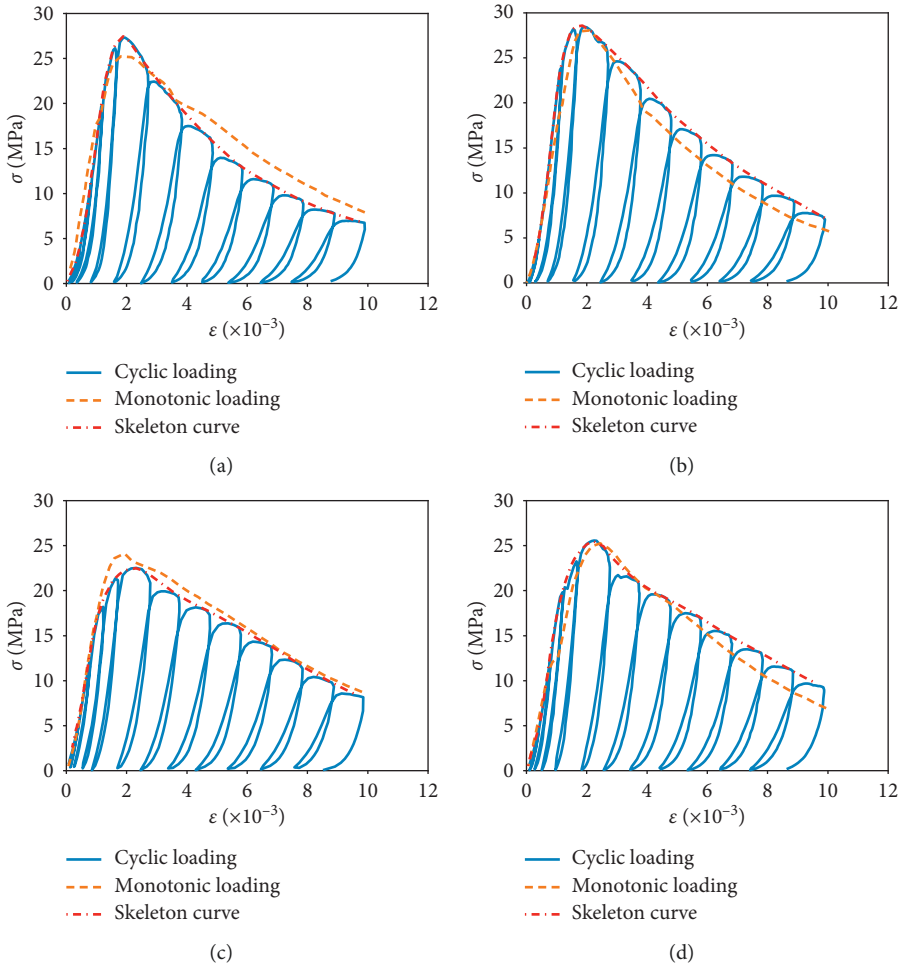

Figure 10: Continued.

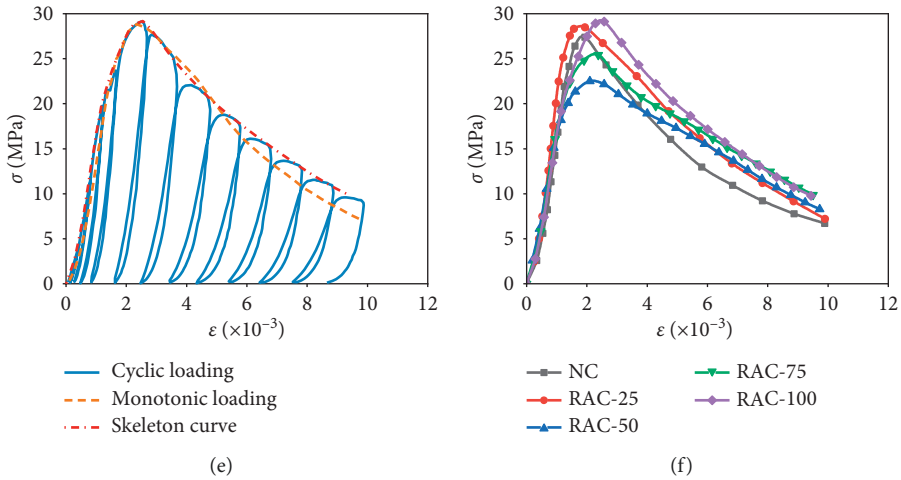

Figure 10: Stress-strain curves of the RAC. (a) NAC. (b) RAC-25. (c) RAC-50. (d) RAC-75. (e) RAC-100. (f) Skeleton curves.

where ε^e and ε^p are the elastic strain and plastic strain, respectively. Let the Helmholtz free energy be defined as [33]

$$\psi = \psi(\varepsilon^e, \kappa, d), \tag{12}$$

where κ is the plastic internal variable and d is the damage variable. According to the second law of thermodynamics, the Clausius–Duhem inequality must be satisfied for the isothermal process:

$$(\sigma \cdot \dot{\varepsilon}) - \dot{\psi} \geq 0. \tag{13}$$

Combing equations (12) and (13), we can have

$$\left(\sigma - \frac{\partial \psi}{\partial \varepsilon^e}\right)\dot{\varepsilon}^e + \left(\sigma\dot{\varepsilon}^p - \frac{\partial \psi}{\partial d}\dot{d}\right) - \frac{\partial \psi}{\partial \kappa}\dot{\kappa} \geq 0. \tag{14}$$

Considering the arbitrariness of $\dot{\varepsilon}^e$, it yields

$$\sigma = \frac{\partial \psi}{\partial \varepsilon^e}. \tag{15}$$

It is assumed that the elastic and plastic Helmholtz free energy are uncoupled [21]; that is, the Helmholtz free energy can be decomposed into the elastic part and the plastic part as follows:

$$\psi(\varepsilon^e, \kappa, d) = \psi^e(\varepsilon^e, d) + \psi^e(\kappa, d), \tag{16}$$

where ψ^e and ψ^p are the elastic part and the plastic part. Thus,

$$\sigma = \frac{\partial \psi}{\partial \varepsilon^e} = \frac{\partial \psi^e}{\partial \varepsilon^e}. \tag{17}$$

Assume the degradation of the Helmholtz free energy of the damaged material can be described by the damage variable d, which is expressed as

$$\psi(\varepsilon^e, \kappa, d) = (1-d)\psi_0(\varepsilon^e, \kappa), \tag{18}$$

where $\psi_0(\varepsilon^e, \kappa)$ is the initial Helmholtz free energy of the material without damage, which can be also decomposed into two parts as

$$\psi_0(\varepsilon^e, \kappa) = \psi_0^e(\varepsilon^e) + \psi_0^p(\kappa), \tag{19}$$

where $\psi_0^e(\varepsilon^e)$ and $\psi_0^p(\kappa)$ are the initial elastic Helmholtz free energy and the initial plastic Helmholtz free energy. The initial elastic Helmholtz free energy equals the elastic strain energy [21]:

$$\psi_0^e(\varepsilon^e) = \int_0^{\varepsilon^e} \sigma d\varepsilon^e = \frac{1}{2}E_0(\varepsilon^e)^2, \tag{20}$$

where E_0 is the initial elastic modulus. Substituting equations (19) and (20) into equations (18) and comparing with equations (16), it yields

$$\psi^e(\varepsilon^e, d) = (1-d)\psi_0^e(\varepsilon^e) = \frac{1}{2}(1-d)E_0(\varepsilon^e)^2. \tag{21}$$

Substituting equations (21) into equations (17), the general uniaxial damaged plastic constitutive relation is formulated as follows:

$$\sigma = (1-d)E_0\varepsilon^e = (1-d)E_0(\varepsilon - \varepsilon^p). \tag{22}$$

3.2. Uniaxial Damaged Plastic Constitutive Equation of the RAC

3.2.1. Description of the Constitutive Equation of the RAC. From the experimental results, the typical stress-strain curve of the RAC under cyclic loading is schematically plotted in Figure 11. At the initial stage of loading, the curve is perfectly linear. As loading continues, the curve bends gradually until the peak point. Beyond the peak point, the stress decreases as the strain increases due to the effect of stress softening. When unloading occurs, the curve proceeds from the unloading point to the residual point located at the strain axis, as shown in Figure 11, and the plastic or residual strain is found upon the completion of unloading.

Since the unloading curve is close to the subsequent reloading curve, as seen in Figure 11, they are both approximated by a line connecting from the unloading point to the residual point. Thereby, the general uniaxial

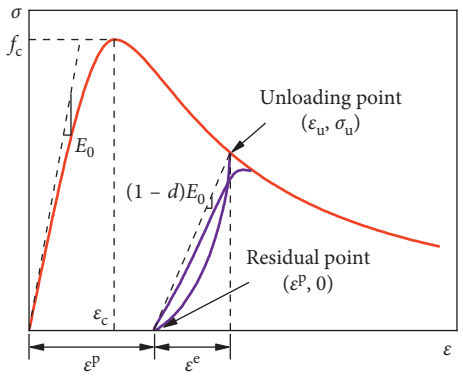

Figure 11: Typical stress-strain curve of the RAC under cyclic loading.

damaged plastic constitutive relation, as expressed in equation (22), can be employed directly to approximately describe the stress-strain relation of the RAC. According to equation (22) as well as Figure 11, the damage variable can be expressed as

$$d = 1 - \frac{E}{E_0}, \tag{23}$$

where E is the modulus of the unloading branch.

For convenience, the stress and strain are expressed in the dimensionless form as follows:

$$x = \frac{\varepsilon}{\varepsilon_c}, \qquad y = \frac{\sigma}{f_c}. \tag{24}$$

Thereby, equation (22) can be rewritten as

$$y = \frac{E_0}{E_s}(1 - d)(x - x^p), \tag{25}$$

where E_s is the secant slope pertaining to the peak point and x^p is the normalized plastic strain, which are expressed, respectively, as

$$E_s = \frac{f_c}{\varepsilon_c}, \qquad x^p = \frac{\varepsilon^p}{\varepsilon_c}. \tag{26}$$

From equation (25), it can be seen that the uniaxial damaged plastic constitutive equation of the RAC can be fully determined provided that x^p and d are given, which are the main tasks in the following two sections.

3.2.2. Plastic Strain Equation of the RAC. According to the experimental results under cyclic loading, the relation between the plastic residual strain and the total strain of the RAC is plotted in Figure 12. It can be found that the plastic strain increases monotonically as the total strain increases. In addition, the RCA replacement percentage has a little

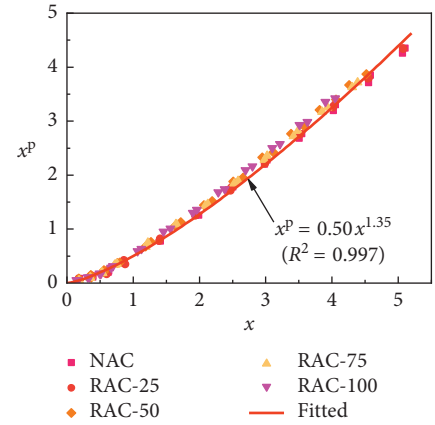

Figure 12: Relation between the plastic strain and the total strain of the RAC.

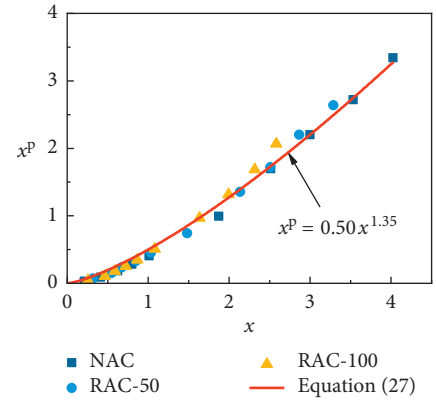

Figure 13: Comparison between the plastic strain and the total strain of the RAC obtained using equation (27) and from reference [34].

effect on the relation. Assume the relation between the plastic residual strain and the total strain is exponential:

$$x^p = mx^n, \tag{27}$$

where m and n are constants to be determined. By fitting the experimental data, it can be obtained that $m = 0.50$ and $n = 1.35$. The fitting curve is also shown in Figure 12. It can be seen that the proposed equation (27) provides very close prediction of the plastic strain.

Figure 13 shows the relation between the plastic strain and the total strain of the RAC obtained from another experiment [34] and the predictions using equation (27). It can be seen that the proposed relation still has a good accuracy.

3.2.3. Damage Evolution Equation of the RAC. For the NAC, Qian and Zhou [35] proposed an empirical damage evolution equation based on the experimental results, in which the damage evolution is described by a continuous smooth piecewise curve. This equation is modified in this study to describe the damage evolution process of the RAC as follows:

$$d = \begin{cases} A_1 x^{B_1}, & 0 < x < 1, \\ 1 - \dfrac{A_2 + B_2 x}{C_2 (x-1)^{D_2} + x}, & x > 1. \end{cases} \tag{28}$$

where A_1, B_1, A_2, and B_2 are the constants which can be determined by the boundary conditions and C_2 and D_2 are the parameters which controls the shape of the stress-strain curve and are determined simply by fitting the experimental data.

Substituting equations (26) and (27) into equations (25) and considering the following boundary conditions at the peak point of the stress-strain curve:

$$\begin{aligned} y|_{x=1} &= 1, \\ \left.\frac{dy}{dx}\right|_{x=1} &= 0. \end{aligned} \tag{29}$$

the values of A_1, B_1, A_2, and B_2 can be determined as

$$\begin{aligned} A_1 &= 1 - \frac{1}{1-m}\frac{E_s}{E_0}, \\ B_1 &= \frac{1-mn}{(1-m)\left[\left((1-m)E_0/E_s\right)-1\right]}, \\ A_2 &= \frac{1-mn}{(1-m)^2}\frac{E_s}{E_0}, \\ B_2 &= \frac{m(n-1)}{(1-m)^2}\frac{E_s}{E_0}. \end{aligned} \tag{30}$$

In addition, according to equation (23) and the experimental data, the values of C_2 and D_2 are obtained through regression analysis as follows:

$$\begin{aligned} C_2 &= 1.46r^2 - 1.16r + 0.71, \\ D_2 &= 1.72. \end{aligned} \tag{31}$$

Figures 14 and 15 show the relation between the damage variable and the total strain obtained in this study and from Liu et al. [34] together with the damage evolution curve, as described in equation (28), of the RAC corresponding to different RCA replacement percentages. It can be seen that, for the RAC, the damage develops slowly until the stress reaches the peak stress. After that, the damage grows rapidly and then tends to slow down as the plastic deformation increases. Overall, the proposed damage evolution equation can well predict the damage evolution process of the RAC under cyclic loading.

4. Verification of the Proposed Constitutive Relation of the RAC

Equation (25) along with equations (27) and (28) forms the fundamental equations for the uniaxial damaged plastic constitutive relation of the RAC. The key material parameters include f_c, ε_c, E_c, and r. Since the two middle parameters can be estimated by the other two ones, as seen in equations (5a), (5b), (7), and (9), the proposed uniaxial damaged plastic constitutive relation can be fully described only by the compressive strength of the RAC and the RCA replacement percentage.

In order to validate the proposed constitutive relation in the monotonic loading scenario, the calculated stress-strain curves of the RAC using the proposed model are compared with the experimental ones obtained in this study and from other scholars [16, 29], as shown in Figure 16. It can be seen that the predictions using the proposed model has a fairly close agreement with the experimental results under monotonic loading.

In addition, verification is also made in cases of cyclic loading. Figures 17 and 18 show the computed stress-strain curves of the RAC using the proposed model and the experiment ones obtained in this study and from Liu et al. [34], respectively. Again, a close agreement has been achieved, indicating that the proposed model can be used to well capture the hysteresis behavior of the RAC under cyclic loading.

5. Application of the Proposed Constitutive Relation of the RAC

In the former sections, the uniaxial damaged plastic constitutive relation of the RAC was proposed and validated using the experimental results. In this section, the proposed constitutive relation of the RAC is programmed into ABAQUS by the UMAT subroutine [36], which is then applied in the nonlinear analysis of the RAC column under cyclic loading. Since the tensile strength of the RAC is a lot smaller than the compressive strength, the tensile behavior of the RAC is neglected for simplification purpose.

A total of four RAC columns involved in the experimental study [37, 38] are selected in the case studies. Figure 19 shows the dimensions and reinforcement details of the RAC columns. The key relevant material properties are listed in Table 4, where f_y and E are the yield strength and elastic modulus of longitudinal rebars, respectively, and N is the axial force. It can be seen that the two columns are almost identical except for the axial force and the RCA replacement percentage.

The column is modeled by the B31 element, and the developed RAC material is adopted. The longitudinal rebar is defined by adding *rebar keywords in the input files, and the elastic-perfectly plastic material is adopted. Note that the effect of stirrups is ignored in the analysis. The computed lateral force vs. displacement curve at the top of the RAC columns is plotted in Figure 20. It can be seen that, compared to specimens RCZ-0 and RCZ-100, specimens NCCC-1 and NCCC-2 have more significant pinching effect due to their smaller slenderness ratios. The computed results can properly reflect this tendency. Overall, the computed results agree well with the test ones, indicating that the proposed damaged plastic constitutive relation of the RAC is capable

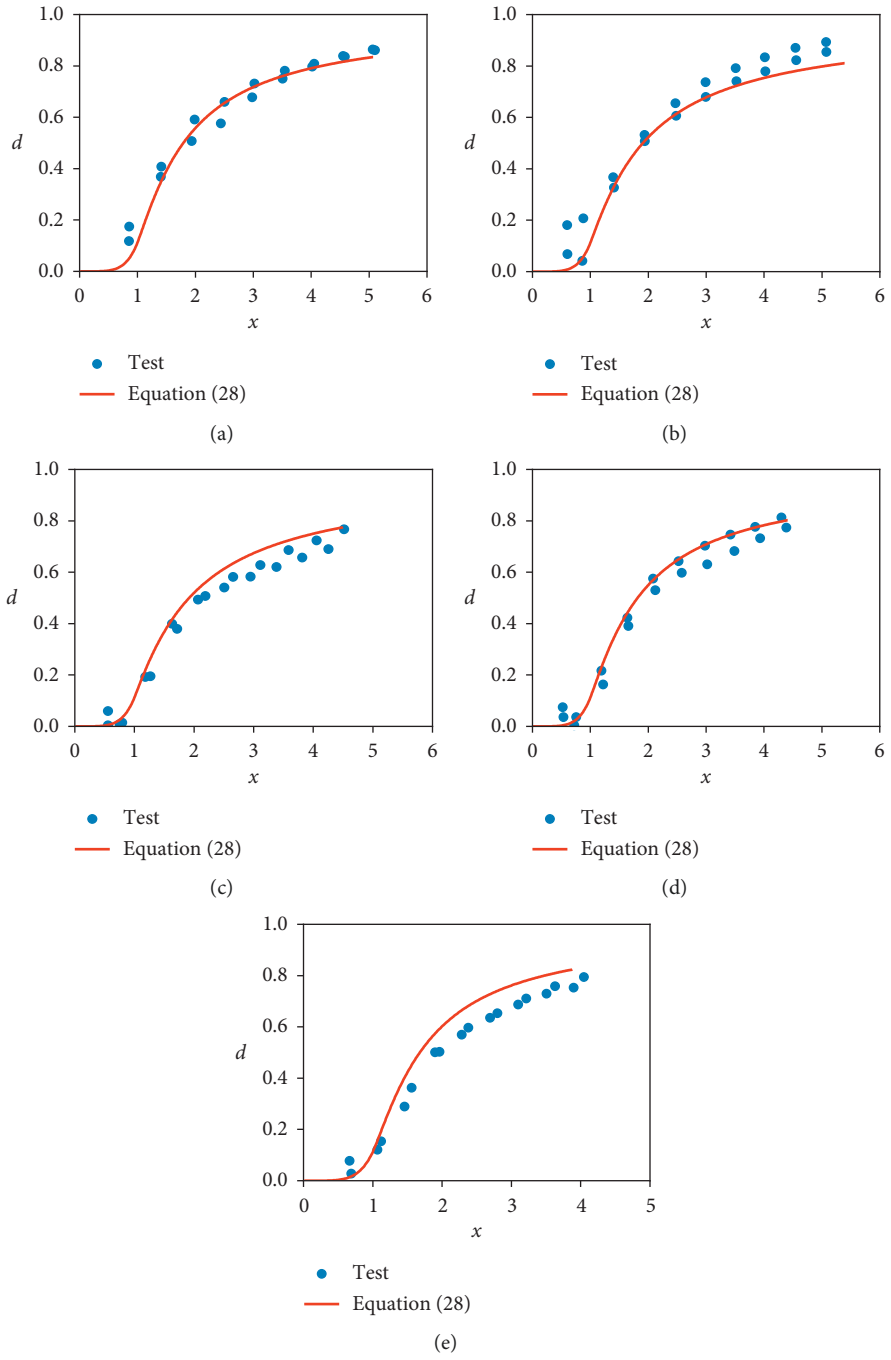

Figure 14: Damage evolution of the RAC in this study. (a) NAC (r = 0). (b) RAC-25 (r = 25%). (c) RAC-50 (r = 50%). (d) RAC-75 (r = 75%). (e) RAC-100 (r = 100%).

of capturing the hysteresis behavior of RAC columns under cyclic loading.

6. Conclusion

In this paper, a total of five groups of RAC specimens with different RCA replacement percentages are tested under both monotonic loading and cyclic loading. Based on the test results, the damaged plastic constitutive relation of the RAC is proposed within the continuous thermodynamics framework. Finally, the proposed RAC constitutive model is programmed into the software ABAQUS to analyze the RAC columns under cyclic loading. Based on this study, the following main conclusions can be drawn:

(1) The peak strain and elastic modulus of the RAC has a good correlation with the compressive strength. The formulae proposed in this study can be used to

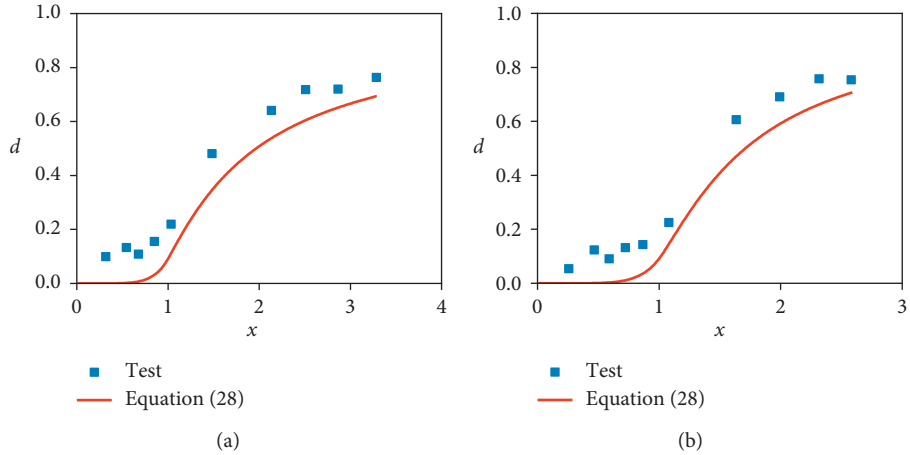

Figure 15: Damage evolution of the RAC obtained from reference [34]. (a) RAC-50 (r = 50%). (b) RAC-100 (r = 100%).

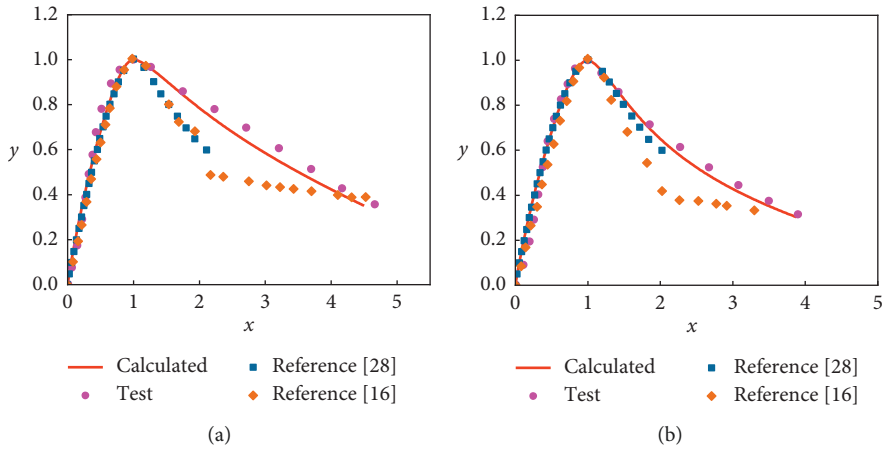

Figure 16: Verification of the proposed model under monotonic loading. (a) r = 50%. (b) r = 100%.

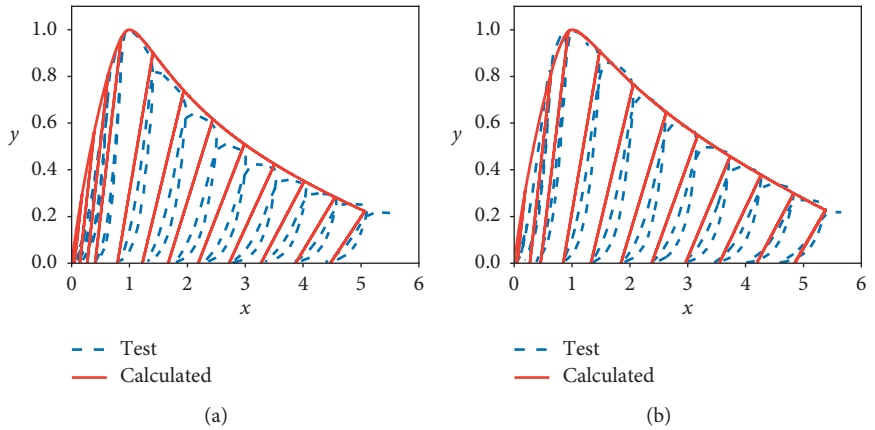

Figure 17: Continued.

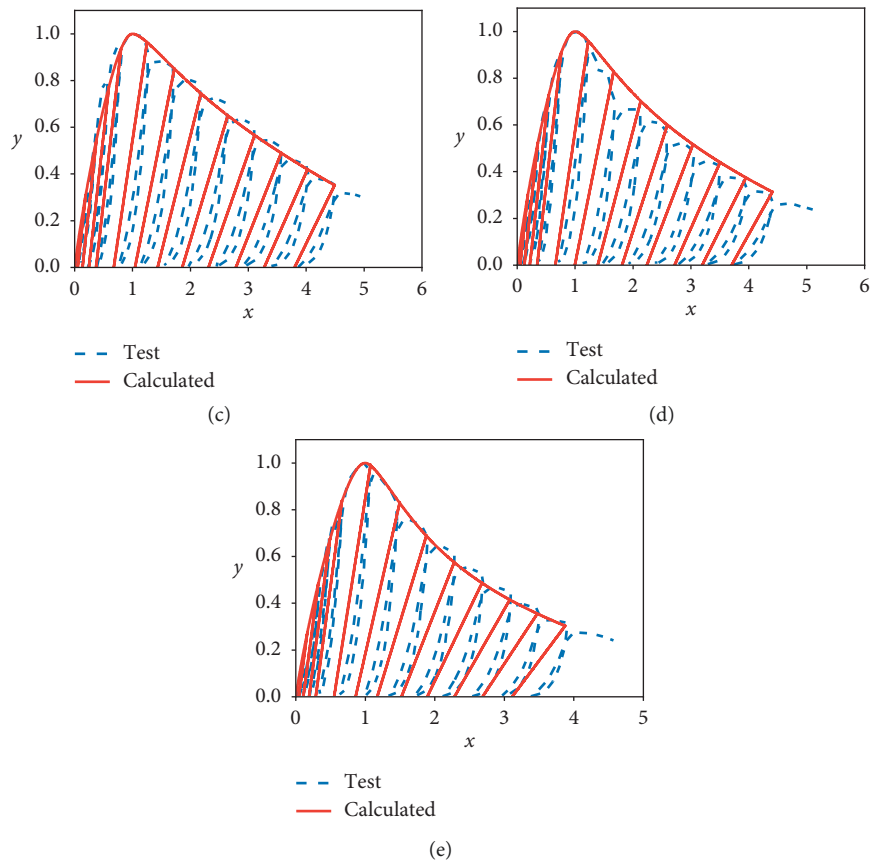

Figure 17: Verification of the proposed model in the case of cyclic loading using the test results in this study. (a) NAC (r = 0). (b) RAC-25 (r = 25%). (c) RAC-50 (r = 50%). (d) RAC-75 (r = 75%). (e) RAC-100 (r = 100%).

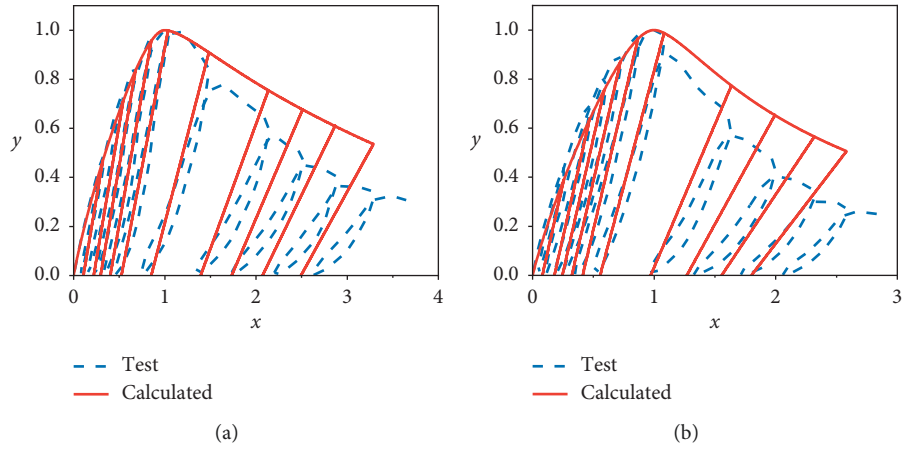

Figure 18: Verification of the proposed model in the case of cyclic loading using the other test results [34]. (a) RAC-50 (r = 50%). (b) RAC-100 (r = 100%).

estimate the peak strain and elastic modulus of the RAC based on the compressive strength and the RCA replacement percentage.

(2) The plastic strain of the RAC is solely dependent on the total strain and irrespective of the RCA replacement percentage. The damage evolution equation proposed in this study, which considers the effect of the RCA replacement percentage, can well describe the damage evolution process of the RAC.

(3) The proposed damaged plastic constitutive relation of the RAC established within the continuous thermodynamics framework has a very simple form,

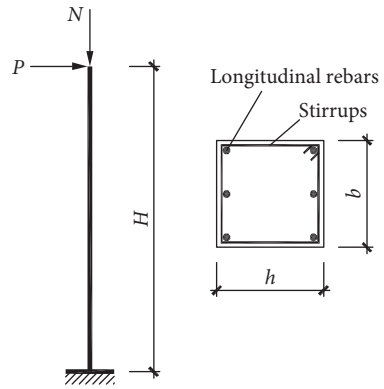

Figure 19: Dimensions and reinforcement details of the RAC columns.

Table 4: Key relevant dimensions and material properties of the columns.

Ref.	Specimen no.	r (%)	f_c (MPa)	N (kN)	f_y (MPa)	E (GPa)	H (mm)	b (mm)	h (mm)	Longitudinal rebars	Stirrups
[36]	NCCC-1	0	30.5	809	353	196	1000	350	350	6⌀16	ϕ8@200
	RCCC-2	100	28.4	754							
[37]	RCZ-0	0	37.2	502	366	200	1100	300	300	4⌀20	ϕ8@50
	RCZ-100	100	33.9	458							

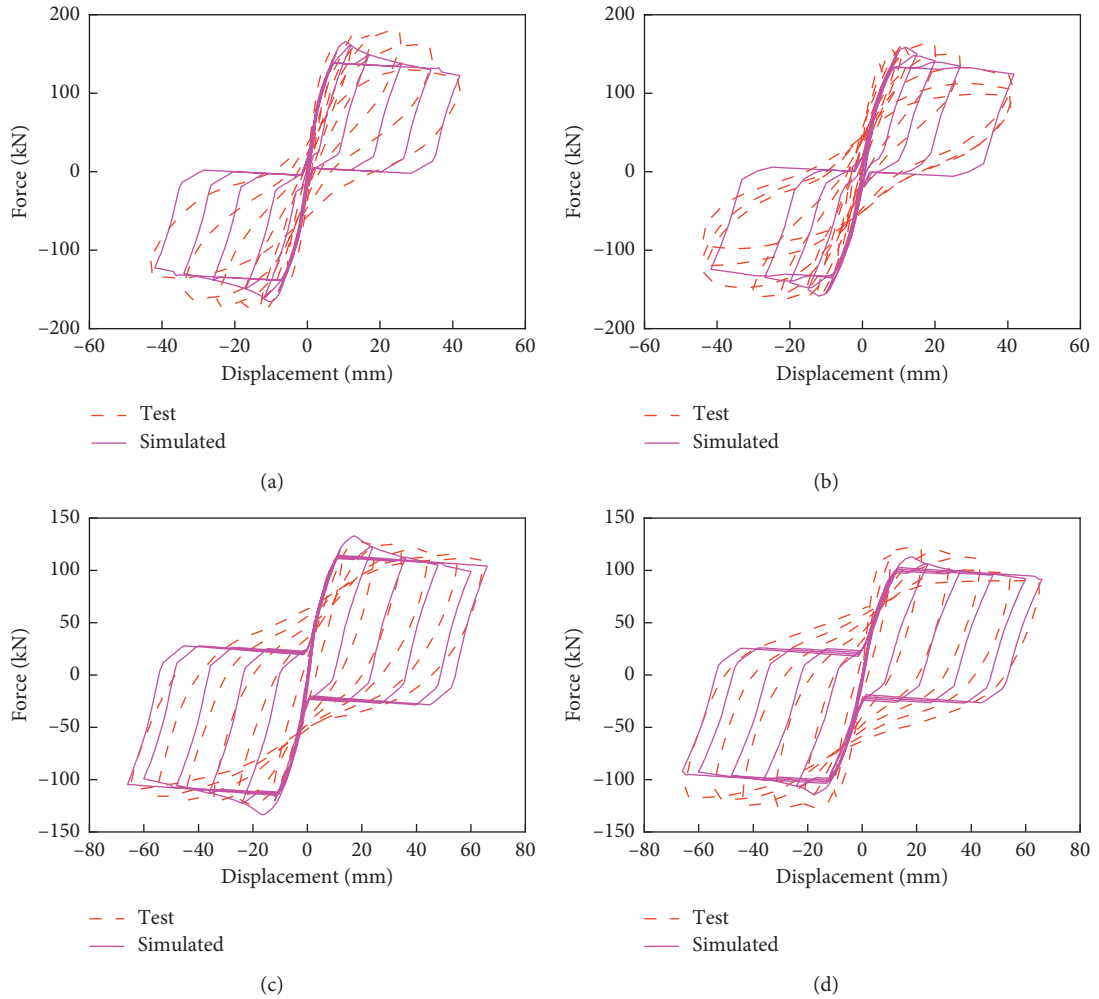

Figure 20: Nonlinear analysis of the RAC columns under cyclic loading. Specimens (a) NCCC-1 (r = 0), (b) RCCC-2 (r = 100%), (c) RCZ-0 (r = 0), and (d) RCZ-100 (r = 100%).

while attaining a good accuracy in capturing the hysteresis behavior of the RAC columns under cyclic loading.

Data Availability

The data used to support the findings of this study are included within the article.

Conflicts of Interest

The authors declare that there are no conflicts of interest regarding the publication of this paper.

Acknowledgments

This paper is part of a project that has received funding from the European Union's Horizon 2020 Research and Innovation Programme under grant agreement no. 777823.

References

[1] J. Xiao, W. Li, Y. Fan, and X. Huang, "An overview of study on recycled aggregate concrete in China (1996–2011)," *Construction and Building Materials*, vol. 31, pp. 364–383, 2012.

[2] R. V. Silva, J. de Brito, and R. K. Dhir, "Properties and composition of recycled aggregates from construction and demolition waste suitable for concrete production," *Construction and Building Materials*, vol. 65, pp. 201–217, 2014.

[3] J. Xiao, W. Li, and C. Poon, "Recent studies on mechanical properties of recycled aggregate concrete in China—a review," *Science China Technological Sciences*, vol. 55, no. 6, pp. 1463–1480, 2012.

[4] I. B. Topçu, "Physical and mechanical properties of concretes produced with waste concrete," *Cement and Concrete Research*, vol. 27, no. 12, pp. 1817–1823, 1997.

[5] J. Xiao, J. Li, and C. Zhang, "Mechanical properties of recycled aggregate concrete under uniaxial loading," *Cement and Concrete Research*, vol. 35, no. 6, pp. 1187–1194, 2005.

[6] A. Akbarnezhad, K. C. G. Ong, M. H. Zhang, C. T. Tam, and T. W. J. Foo, "Microwave-assisted beneficiation of recycled concrete aggregates," *Construction and Building Materials*, vol. 25, no. 8, pp. 3469–3479, 2011.

[7] I. Martínez-Lage, F. Martínez-Abella, C. Vázquez-Herrero, and J. L. Pérez-Ordóñez, "Properties of plain concrete made with mixed recycled coarse aggregate," *Construction and Building Materials*, vol. 37, pp. 171–176, 2012.

[8] M. Breccolotti, A. D'alessandro, F. Roscini, and M. Federico Bonfigli, "Investigation of stress-strain behaviour of recycled aggregate concrete under cyclic loads," *Environmental Engineering and Management Journal*, vol. 14, no. 7, pp. 1543–1552, 2015.

[9] J. Andal, M. Shehata, and P. Zacarias, "Properties of concrete containing recycled concrete aggregate of preserved quality," *Construction and Building Materials*, vol. 125, pp. 842–855, 2016.

[10] M. Etxeberria, E. Vázquez, A. Marí, and M. Barra, "Influence of amount of recycled coarse aggregates and production process on properties of recycled aggregate concrete," *Cement and Concrete Research*, vol. 37, no. 5, pp. 735–742, 2007.

[11] S. Manzi, C. Mazzotti, and M. C. Bignozzi, "Short and long-term behavior of structural concrete with recycled concrete aggregate," *Cement and Concrete Composites*, vol. 37, no. 1, pp. 312–318, 2013.

[12] Z. H. Deng, L. Chen, J. Qian, and C. L. Meng, "Experimental study on stress-strain curve of recycled coarse aggregate concrete under uniaxial compression," *Applied Mechanics and Materials*, vol. 357–360, pp. 1415–1419, 2013.

[13] N. Y. Ho, Y. P. K. Lee, W. F. Lim et al., "Efficient utilization of recycled concrete aggregate in structural concrete," *Journal of Materials in Civil Engineering*, vol. 25, no. 3, pp. 318–327, 2013.

[14] Á. Salesa, J. A. Pérez-Benedicto, D. Colorado-Aranguren et al., "Physico–mechanical properties of multi–recycled concrete from precast concrete industry," *Journal of Cleaner Production*, vol. 141, pp. 248–255, 2017.

[15] C. Zhou and Z. Chen, "Mechanical properties of recycled concrete made with different types of coarse aggregate," *Construction and Building Materials*, vol. 134, pp. 497–506, 2017.

[16] W. Wang, L. Zhao, Y. Liu, and Z. Li, "Mechanical properties and stress-strain relationship in axial compression for concrete with added glazed hollow beads and construction waste," *Construction and Building Materials*, vol. 71, pp. 425–434, 2014.

[17] S. Laserna and J. Montero, "Influence of natural aggregates typology on recycled concrete strength properties," *Construction and Building Materials*, vol. 115, pp. 78–86, 2016.

[18] N. K. Bairagi, K. Ravande, and V. K. Pareek, "Behaviour of concrete with different proportions of natural and recycled aggregates," *Resources, Conservation and Recycling*, vol. 9, no. 1-2, pp. 109–126, 1993.

[19] X. Li, "Recycling and reuse of waste concrete in China: part I. Material behaviour of recycled aggregate concrete," *Resources, Conservation and Recycling*, vol. 53, no. 1-2, pp. 36–44, 2008.

[20] J. Mazars, "A description of micro-and macroscale damage of concrete structures," *Engineering Fracture Mechanics*, vol. 25, no. 5-6, pp. 729–737, 1986.

[21] J. W. Ju, "On energy-based coupled elastoplastic damage theories: constitutive modeling and computational aspects," *International Journal of Solids and Structures*, vol. 25, no. 7, pp. 803–833, 1989.

[22] J. Lubliner, J. Oliver, S. Oller, and E. Oñate, "A plastic-damage model for concrete," *International Journal of Solids and Structures*, vol. 25, no. 3, pp. 299–326, 1989.

[23] R. Faria, J. Oliver, and M. Cervera, "A strain-based plastic viscous-damage model for massive concrete structures," *International Journal of Solids and Structures*, vol. 35, no. 14, pp. 1533–1558, 1998.

[24] X. Hu, Q. Lu, Z. Xu, W. Zhang, and S. Cheng, "Compressive stress-strain relation of recycled aggregate concrete under cyclic loading," *Construction and Building Materials*, vol. 193, pp. 72–83, 2018.

[25] JGJ52-2006, *Standard for Technical Requirements and Test Method of Sand and Crushed Stone (or Gravel) for Ordinary Concrete*, China Architecture & Building Press, Beijing, China, 2006, in Chinese.

[26] DG/TJ08-2018-2007, *Technical Code on the Application of Recycled Concrete*, Shanghai Construction and Transportation Committee, Shanghai, China, 2007, in Chinese.

[27] M. C. Limbachiya, "Coarse recycled aggregates for use in new concrete," *Engineering Sustainability*, vol. 157, no. 2, pp. 99–106, 2004.

[28] I. González-Taboada, B. González-Fonteboa, F. Martínez-Abella, and D. Carro-López, "Study of recycled concrete aggregate quality and its relationship with recycled concrete

compressive strength using database analysis," *Materiales de Construcción*, vol. 66, no. 323, p. e089, 2016.

[29] G.-F. Belén, M.-A. Fernando, C. L. Diego, and S.-P. Sindy, "Stress-strain relationship in axial compression for concrete using recycled saturated coarse aggregate," *Construction and Building Materials*, vol. 25, no. 5, pp. 2335–2342, 2011.

[30] M.-D. Nguyen, G. Wardeh, and E. Ghorbel, "Mechanical behavior of recycled aggregate concrete under uniaxial loading-unloading cycles," in *Proceedings of the 10th International Conference on Mechanics and Physics of Creep, Shrinkage, and Durability of Concrete and Concrete Structures (CONCREEP 10)*, Vienna, Austria, September 2015.

[31] BS EN 1992-1-1, *Eurocode 2: Design of Concrete Structures-Part 1-1: General Rules and Rules for Buildings*, Comite Europeen de Normalisation (CEN), Brussels, Belgium, 2004.

[32] GB50010-2010, *Code for Design of Concrete Structures*, China Architecture & Building Press, Beijing, China, 2010, in Chinese.

[33] J. Lemaitre, "How to use damage mechanics," *Nuclear Engineering and Design*, vol. 80, no. 2, pp. 233–245, 1984.

[34] K. Liu, J. Yan, C. Zou, and H. Wu, "Cyclic stress-strain model for air-entrained recycled aggregate concrete after freezing-and-thawing cycles," *ACI Structural Journal*, vol. 115, no. 3, pp. 711–722, 2018.

[35] J. C. Qian and J. F. Zhou, "Two concrete damage models and their application," *Journal of Hohai University*, vol. 17, no. 3, pp. 40–47, 1989, in Chinese.

[36] Dassault-Systèmes, *Abaqus User Subroutine Reference Guide*, 2014, http://abaqus.software.polimi.it/v6.14/books/sub/default.htm.

[37] J. Xiao, X. Huang, and L. Shen, "Seismic behavior of semi-precast column with recycled aggregate concrete," *Construction and Building Materials*, vol. 35, pp. 988–1001, 2012.

[38] G. Bai, C. Liu, H. Zhao et al., "Experimental research on seismic behavior of recycled concrete frame columns," *Journal of Earthquake Engineering and Engineering Vibration*, vol. 31, no. 1, pp. 61–66, 2011, in Chinese.